# Nanoscale

# Journal Name

# Structure vs excitonic transitions in self-assembled porphyrin nanotubes and their effect on light absorption and scattering

Oriol Arteaga,[*a] Adolf Canillas,[a] Zoubir El-Hachemi[b], Joaquim Crusats[b], Josep M. Ribó[b]

The optical properties of diprotonated *meso*-tetrakis(4-sulphonatophenyl)porphyrin (TPPS$_4$) J-aggregates of elongated thin particles (nanotubes in solution and ribbons when deposited on solid interfaces) are studied by different polarimetric techniques. The selective light extinction in these structures, which depends on the alignment of the nanoparticle with respect to the polarization of light, is contributed by excitonic absorption bands and by resonance light scattering. The optical response as a function of the polarization of light is complex because, although the quasi-one-dimensional structure confines the local fields along the nanotube axis, there are two orthogonal excitonic bands, of H- and J- character, that can work in favor or against the field confinement. Results suggest that resonance light scattering is the dominating effect in solid state preparations, i.e. in collective groups (bundles) of ribbons but, in diluted solutions, i.e. with isolated nanotubes, the absorption at the excitonic transitions remains dominant and linear dichroism spectra can be a direct probe of the exciton orientations. Therefore, by analyzing scattering and absorption data we can determine the alignment of the excitonic bands within the nanoparticle, i.e. of the orientation of the basic 2D porphyrin architecture in the nanoparticle. This is a necessary first step for understanding the directions of energy transport, charge polarization and non-linear optical properties in these materials.

## 1 Introduction

J-aggregates are supramolecular structures obtained by self-assembly which show photo-electronic properties of theoretical and applied interest[1–3], for example they are biomimetic systems for light harvesting antennas. However, there is a lack of knowledge of the electronic ordering in their mesoscopic structures. This represents a problem to understand their opto-electronic or energy transport properties and a hindermost in the progress towards potential applications.

An interesting group of J-aggregates is obtained by self-assembly of the diprotonated forms of *meso*-substituted amphiphilic porphyrins, being the most representative member of this series the *meso*-tetrakis(4-sulphonatophenyl)porphyrin (TPPS$_4$). Despite the porphyrin building blocks are achiral, the self-assembled J-aggregates show an intrinsically chiral structure

that leads to chiral electronic transitions, i.e. to circular dichroism at the corresponding electronic transitions. The electronic and optical properties of the porphyrin are drastically modified as a result of its self-assembly into a supramolecular species, because dipole-dipole interaction among the constituent molecules cause an energy shift of the absorption bands compared to the monomer and the transfer of the local excitation to form an Frenkel exciton, i.e the charge separation in the electronic transition through many dipole-dipole interacting porphyrins. Furthermore, the homogeneous ordering of these oscillators within a nanoparticle yields an oscillator coupling between a large number of excitons[4,5].

There are two types of excitonic coupling between the porphyrin monomer units: the so-called J-bands, consequence of the side-to-side coupling of transition dipoles, showing a red shift of the Soret- and Q-bands of the porphyrin (489 nm and 707 nm, respectively, compared to 433 nm and 644 nm of the monomer) and, also, a blue-shifted Soret band ($\sim$ 420nm), called H-band, that is characteristic of porphyrin face-to-face coupling ($\pi$-stacking). Currently, there is an increasing interest in the study of the role H- and J- excitonic interactions in soft-matter light harvesting system[6,7] and for potential opto-electronic aplications[8].

[a] *Dep. Física Aplicada i Òptica, C/ Martí i Franquès, Universitat de Barcelona, 08028, Barcelona, Catalonia, Spain. ; Tel: 34 934039221; E-mail: oarteaga@ub.edu*
[b] *Dep. Química Orgànica, Institute of Cosmos Science (IEEC-UB), C/ Martí i Franquès, Universitat de Barcelona, 08028, Barcelona, Catalonia, Spain*
† Electronic Supplementary Information (ESI) available: [details of any supplementary information available should be included here]. See DOI: 10.1039/b000000x/
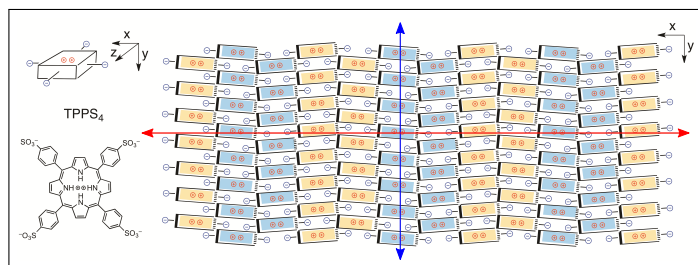
**Fig. 1** Porphyrin architecture on a plane. The excitons are shown by the double headed arrows (H-exciton, blue; J-exciton, red).

Recently, the structure of a chiral porphyrin mosaic sheet of TPPS$_4$ J-aggregates has been revealed by diffraction techniques[9]. This structure, shown in Fig. 1, takes into account the orthogonality between J- and H- excitonic bands, which was experimentally inferred in previous reports[10,11].The nanoparticles of the TPPS$_4$ J-aggregates show different morphologies that can be formed by mono-, bi- or multilayered structures. The most interesting ones assemble in long and thin structures that in the solution are hollow, single-walled nanotubes[12–14] and when deposited on dry substrates collapse into bilayered ribbons. We use an experimental procedure adapted from ref. 14 that allows the preparation of solutions containing only nanotubes and, therefore, it is possible to asses that the optical properties of these samples correspond to a specific group of mesoscopic forms, i.e. nanotubes in the solution and ribbons by solution casting at solid/air interface.

The porphyrin monomers self-assemble into the 2D sheet of Fig. 1. This sheet is flexible enough to roll into a nanotube when the aggregation achieves the adequate length, in a similar way that a graphene sheet would wrap into single walled carbon nanotube[§]. The orientation of the J- and H-excitons with respect to the nanotube axis depends, actually, on the rolling direction. The objective of this paper is to verify experimentally the nature and orientation of these transitions in the nanoparticles by means of polarimetric methods that study the absorption and scattering contributions to the nanotube extinction properties. We find that the overall optical response arises from the reduced dimensionality of the particles combined with the excitonic bands that are embedded in their structure. These results also allow for a better understanding of the chiro-optical phenomena resulting from the stirring-induced deformations of the nanotubes.

## 2 Experimental

### 2.1 Polarimetric measurements

Polarimetric measurements were made with two different instruments: a spectroscopic Mueller matrix polarimeter based on four photoelastic modulators[15] and a Mueller matrix microscope based on the continuous dual rotating compensator technique[16]

(further experimental details are available in the Supporting Information). The first instrument was used to analyze solutions containing TPPS$_4$ nanotubes, both in transmission and scattering configurations using a 10 mm pathlength cuvette. The microscope was used to study solid-state preparations of the same substances in which it was possible to observe ribbon bundles. Narrow bandpass filters at 500 nm and 420 nm were used in the microscope to study, respectively, the J-excitonic and H-excitonic transitions. Mueller matrix data was analyzed using the analytic inversion method[17] to calculate, among others, the linear extinction (LE) of the samples. Here we will report LE as the difference between horizontal and vertical extinction in the instrument coordinate system, moreover the component at 45° is also measured, so it is possible to recover the absolute direction of extinction. We use the terminology *linear extinction*, instead of the more common term linear dichroism (LD), because LD refers only to the differential absorption of light for two orthogonal polarizations, while we assume that LE is more general and can include both the scattering and the absorption contributions.

### 2.2 Sample preparation

The solutions of J-aggregate nanoparticles were prepared by injecting 250 $\mu$l of a mother solution of the diprotonated porphyrin hydrochloride form TPPS$_4$.2HCl (2 mM − 8 mM of zwitterionic porphyrin according to Ref. 18) to 1 ml of HCl 0.01M. The procedure leading to solutions composed quasi-exclusively of straight particles (ribbon/nanotubes) was adapted from Ref. 14 and it is based on the slow injection of mother solution using a capillary needle (Hamilton syringe, 0.7 mm external diameter needle, injection time 5 s) to the inner of the acid water solution. The mother solutions were prepared from the hydrochloride porphyrin equilibrated for 24 hours or from fresh eluted concentrate solutions of the zwitterionic porphyrin prepared by column ion exchange (protonated form) of the porphyrin tetrasodium salt free of salts. More common preparation methods in which the mother solution is added to the acid solution under gentle stirring, lead to solutions containing a relatively high proportion of straight nanoparticles but also a significant amount of round small particles and plate-like particle.

Films for Mueller matrix microscopy where prepared from concentrate solutions showing only long straight particles ( > 1 $\mu$m). Solution drops were deposited on an inclined glass slide in order to obtain some alignment between the nanoparticle bundles. They were left to dry at room temperature and humidity conditions.

Diluted solutions for optical measurements in 1 cm path length cuvettes were obtained by the dilution of 7 $\mu$l of the above described nanotube solutions in 1250 $\mu$l 0.01 M HCl, 0.4 M NaCl water solution. The dilution in acidic solution (pH 2) in the absence of NaCl would lead to the slow deaggregation of the porphyrin aggregates. The stability of the nanotubes in this dilution procedure was controlled by Peak Force Microscopy (PFM). PFM methods are described in the Supporting Information.

---

§ Recent diffraction results[9,14] show that the porphyrin rings are coplanar with the monolayer. The closing of the sheet structure of Fig. 1 into a nanotube must imply some structural relaxation. However, the structural modification in the transition from a planar nanoparticle to a nanotube is probably not very significant because it is not detected by changes in the UV/Vis absorption spectra (using routine spectrometric techniques).

## 2.3  Nanotubes vs nanoribbons

When the solution with nanotubes is deposited on a dry solid substrate and the surrounding bulk water is eliminated the nanotubes collapse to bilayered ribbons as it is shown in Fig. 2. This morphology variation leads to a change from the elastic behavior of the isolated nanotubes in diluted solution to a plastic behavior of the bilayered ribbons. Details on this will be published elsewhere. As the bilayered ribbons originate from the collapse of a single nanotube, their two superposed layers must exhibit the same architecture and orientation.
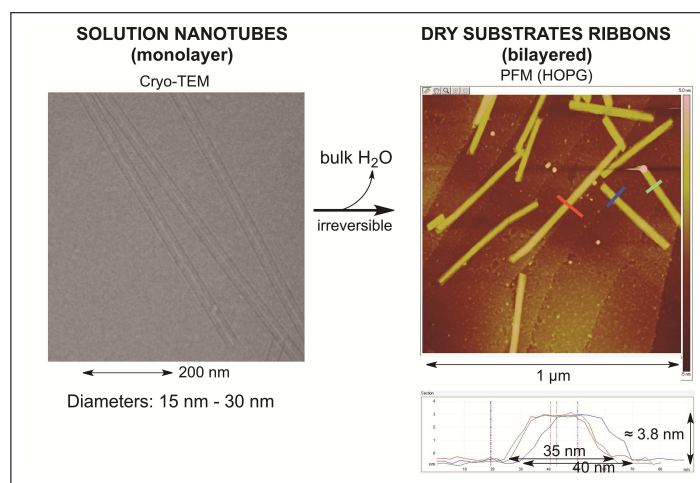


**Fig. 2** Transition from hollow single wall nanotubes seen from the Cryo-electron microscopy image to ribbons when deposited in dry substrates (solid/air interface) as observed in the PFM image.

## 3  Results

Rayleigh scattering is normally not considered for nanoscale objects because it is expected to be extremely weak[19]. However there is a resonant enhancement when the photon energy matches or is near an electronic transition and this effect is very strong when there is an intense coupling among the chromophore units[4,19], as it is characteristic for the TPPS$_4$ family of J-aggregates. Resonance light scattering (RLS) is well known to be strong for aggregates with large volume[4,19], and it can be further enhanced when thin nanoparticles assemble into bundles. Bundling occurs due to side-by-side interactions between the highly polarized porphyrin walls, leading to bundles of aligned nanotubes in which the LE effects increase with the thickness of the bundle, as it is shown in Fig. 3. The linear extinction at 500 nm is very strong and it is clearly oriented along the axis of the ribbon bundles (Fig. 3). This result is in agreement with near field polarized microscopy measurements recently reported in ref. 20. At 420 nm the linear extinction becomes much weaker (is reduced by a factor $\sim 10$, as shown in Fig. 3c), but it has the opposite sign with respect to the result at 500 nm because, in this case, it is oriented perpendicular to the ribbon axis. .

The results in Fig. 3 showing that, for the J-aggregate transition, maximum extinction occurs for light parallel to the axes of the ribbon bundles, could be indicative that the J-transitions are parallel to the nanotube axis. However this picture is not neces-

sarily correct, because we have to consider that, in the observed bundles, RLS and not absorption is the predominant contribution to the extinction. The cross section of scattering[19] is given by

$$\sigma_{sca} = \frac{k^3}{6\pi}|\alpha|^2 = \frac{k^3}{6\pi}(\alpha_r^2 + \alpha_i^2), \qquad (1)$$

where $k$ is the wavevector of light, $k = 2\pi/\lambda$, and $\alpha_r$ and $\alpha_i$ are, respectively, the real and imaginary parts of the polarizability of the aggregates. Note that for nanotubes the scattering cross section scales as the third power of the wavevector, while for spherical particles it scales as the fourth power[21]. The absorption cross section is

$$\sigma_{abs} = k\alpha_i, \qquad (2)$$

so, unlike the scattering cross-section, only depends on the imaginary part of the polarizability.

LE arises due to anisotropy in the polarizability of the porphyrin nanoparticles. This anisotropy can be contributed by two different factors, first by the relative orientations of the J-excitons and H-excitons in the porphyrin sheet, but also by the quasi one-dimensional nature of the particle, that introduces a strong shape-induced anisotropy. For example, the strong scattering efficiency for light polarized along the nanotube axis is a well-known characteristic of carbon nanotubes[22–24]; while, on the other hand, light polarized perpendicular to the nanotube axis losses efficiency because its polarizability is significantly reduced due to screening. This local-field or "antenna effect" strongly reduces the response whenever the electric-field vector of the optical radiation lies perpendicular to the nanotube. Interestingly, if J-excitons are perpendicular (or near perpendicular if chiral closing occurs), they act as very efficient charge transporters, screening this perpendicular polarized radiation by allowing charges to build up at each side of the nanotubes as it is schematically represented in Fig. 4a. Likewise, H-excitons only allow charge transfer in the axial direction, and the charge builds up only at the ends of the nanotube and the screening is much less intense (4b). This excitonic arrangement occurs if the porphyrin sheet in Fig. 1 rolls along the $x$ direction.

To understand better the contributions of absorption and scattering to the extinction we performed spectroscopic transmission and scattering measurements in a diluted solution (where the nanotubes can be considered to be isolated one to another). Scattered light could be detected in a rather broad range from approximately 410 nm to 540 nm (Fig. 5 top). The extinction bands measured in a transmission experiment for this same solution (Fig. 5 bottom) show the two well distinctive orthogonal J-aggregate and H-aggregate peaks, but they are clearly narrower than for the solid state sample. This is suggesting that transmission experiments in solution are mainly probing the absorption contribution (narrow peaks) because, if the light lost by scattering was the dominating contribution to the total extinction, broadened peaks should be expected also in transmission. Absorption peaks are narrow because they depend only on the imaginary part of the polarizability, but the scattering loses also depend on the real part of the polarizability that behaves anomalously in the vicinity of an absorption band, leading to broadened
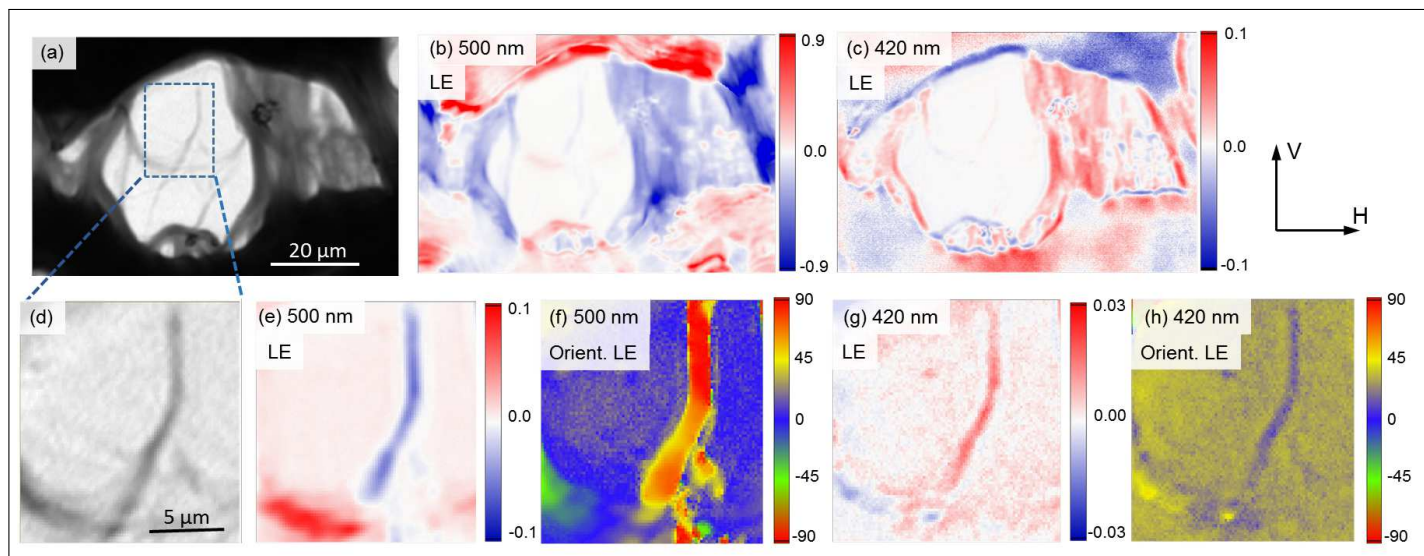
**Fig. 3** Polarimeric images of the ribbon bundles casted on a glass slide measured with the Mueller matrix microscope. The intensity of transmitted light is shown in (a). The LE (horizontal, H or x, minus vertical, V or y, polarizations) shows opposite signs at 500nm (b) and 420 nm (c). A detail of a thinner bundle is shown in (d), together its corresponding LE at 500 nm (e) and at 420 nm (g). Panels f and h show the calculated orientations (in degrees) of maximum LE. At 500 nm the extinction takes place along the bundle axes while at 420 nm it is orthogonal.

spectral peaks and to a small energy shift. This is the reason why the negative J-excitonic band is broadened in solid state and slightly blue-shifted, while the positive H-band is red-shifted.

It is also interesting to observe that there appears to be an anomalous behaviour in the scattering measurement (Fig. 5, top) between 475 nm and 515 nm. This is the interval of wavelengths where the J-aggregate absorption appears to be dominant (LE $\simeq$ LD) in the diluted solutions. The 90° scattering configuration favors the scattering of vertically polarized light at all wavelengths (since scattering always produces linearly polarized light perpendicular to the scattering plane) but, in this interval range, the scattering experiment is also affected by the fact that the solution is absorbing more vertical polarization than horizontal, in agreement with the sign of LE measured in transmission. As it will be discussed later, this is related with the orientation taken by the nanotubes inside the cuvette due to unavoidable vertical convention flows induced by small temperature differences.

## 4 Discussion

Polarimetry measurements suggest that the optical response of the solid preparations is governed by the scattering contribution while, in diluted solutions, absorption is dominant. The reason for the different behaviour between the solid samples and solutions has to be related with the presence of bundles and perhaps favored by the bilayered character of the ribbons compared to the monolayered nanotubes. Bundling perturbs the electronic structure of the nanotubes or ribbons due to side-by-side interaction between the highly polarized porphyrin sidewalls. Studies in single walled carbon nanotubes[25] have shown that bundling produces an enhanced screening of the intratube Coulomb interaction (Fig. 4) and an intertube exciton tunneling. All this leads to a stronger antenna effect. No such effects are possible in the studied solutions because they contain isolated nanotubes with
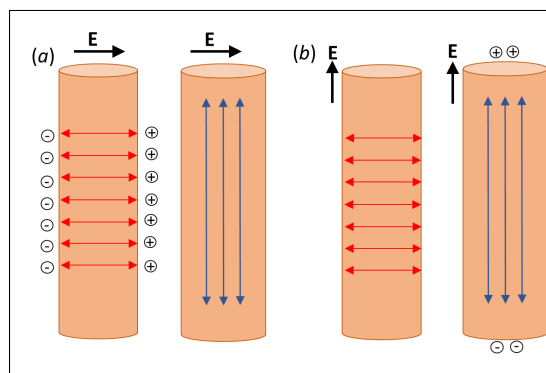


**Fig. 4** Enhanced field screening due to the J-exciton for a electric field perpendicular to the nanotube axis (a). When the electric field is parallel to the nanotube axis positive charges (holes) or negative charges (electrons) can only accumulate at the ends of a nanotube and the J-exciton does not contribute to the charge transfer (b). An analogous scheme holds for bilayered ribbons formed from nanotube collapsing.
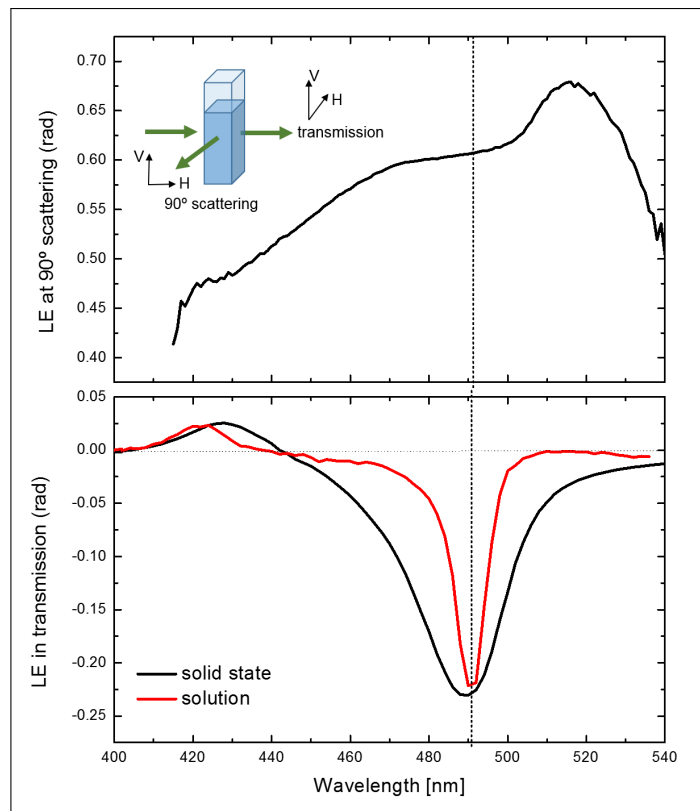
**Fig. 5** Top, LE for the $90°$ scattering of a solution of porphyrin aggregates (nanotubes). Bottom, LE for the same solution in transmission and compared with the LE of a solid sample (data corresponding to the solution has been scaled by a factor $\sim 10$ to reach the same magnitude than in solid state). The anomalous decrease of the scattering LE around 490 coincides with the J-aggregate band, which is only sharp for the transmission measurement in the solution.

diameters between 15 nm and 30 nm . The polarizability ($\alpha$) of the elongated aggregates scales linearly with their volume and therefore, according to Eq. (1), the amount of scattering will depend on the square of the volume of the aggregate, while the absorption will scale linearly. Therefore, the RLS efficiency will strongly depend on the particle size. We conclude that the larger concentration of extended aggregates in the solid state preparations, which is further enhanced by the strong bundling between particles, leads to much stronger RLS effects than in diluted solutions.

In previous reports we have shown that, for this type of supramolecular aggregates, there is a chiral sign induction by the effect of hydrodynamic torques[11,26,27]. The main characteristic of those experiments is that switching the swirling direction inverts the circular dichroism (CD) spectra (Fig. 6c). To explain this phenomenon is necessary to relate the sign of the hydrodynamic torque in the region of measurement with the orientation of the nanotube in the flow as well with the ordering of the excitonic bands in the nanotube. Here we discuss only the orientation of the excitons in the nanotube as originated by the closing of the basic sheet of the J-aggregate structure (Fig. 1). A complete discussion on the origin of the transient CD signal originated by the stirring vortex derived will be published elsewhere. Under the stirring vortex, the magnitude of LE increases with respect to stagnant conditions (Fig. 6a) and the J-exciton band takes negative LE values. This result, together with the analysis of the velocity gradients occurring at the central region of the cuvette (where the spectra was recorded) allowed us to infer that nanotubes had to be predominantly standing horizontal (i.e. orthogonal to the cuvette axis) in the vortex flow. In the diluted nanotube solutions, even when absorption is the main contribution to the extinction, resonant scattering measurements still offer an alternative way to check for the orientation. To assess this, we repeated the $90°$ measurement scheme of Fig. 5 but under clock-wise (CW) and counter-clock wise (CCW) stirring conditions. The results are given in Fig. 6b. Here, contrary to what happened in transmission, the magnitude of linear extinction decreased when stirring. The theory of light scattering from a thin cylinder states that the scattering is more efficient when the incoming polarization is parallel to the cylinder axis, i.e. a cylinder standing horizontally in the cuvette should scatter more horizontal polarization than vertical. Hence, less vertically polarized light reaches the detector, leading to the negative (i.e. decreasing) contribution to the linear extinction that we observe when stirring. These observations confirm that the nanotubes stand horizontal under gentle vortex stirring.

The differential circular extinction at $90°$ scattering for CW and CCW stirring is shown in Fig. 6d. The sign of the characteristic bisignated bands are opposite to those observed for transmission (Fig. 6c). This result is not too surprising, since it means that, if for example, with CW stirring left- CPL has the highest extinction in transmission, scattered light will show a predominant lack (i.e. extinction) of right- CPL since this is the handedness that is more transmitted through the sample. In this case we can also observe that the scattering bands are broader than their transmission counterparts. This is another indication that absorption, and
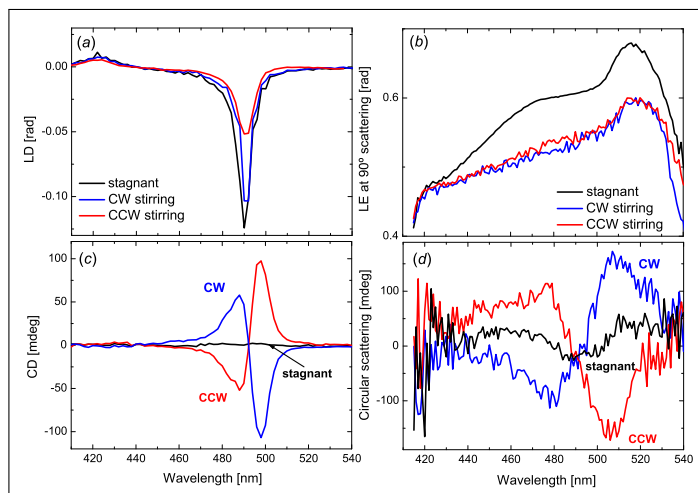
**Fig. 6** Comparison of linear and circular anisotropies of a nanotube solution under stirring and stagnant conditions. (a) shows that there is an increase of LD in the transmission measurement when stirring, while (b) shows an analogous comparison but in the terms of the LE observed for 90° scattering. (c) shows the induction of opposite patterns of CD for clock-wise (CW) and counter clock-wise (CCW) stirring. (d) shows the differential circular scattering for CW and CCW stirring measured at the 90° scattering configuration.

not differential light scattering, is the main contribution the CD signals observed in transmission.

Our measurements confirm that the predominant orientation of the nanotubes is horizontal in the stirring vortex and with the H-excitonic band oriented axially and the J-excitonic band radially. This is in agreement with the primordial sheet rolling into a nanotube through the J direction, as we had anticipated from the microscopy measurements. This rolling direction probably yields the more stable structure because it is the principal direction where the electrostatic, hydrogen bonds and hydrophobic effects act to form the J-aggregate [3]. The axial direction is originated by weaker $\pi$-stacking forces but, as it is common in self-assembly and in the crystallization of flat organic compounds, it corresponds to the direction of faster growth. In fact, nanotube ripening and growth at expenses of monomeric and small J-aggregate particle transform after some weeks short nanotubes (100 nm – 300 nm) in several $\mu$m long nanotubes of the same diameter.

## 5 Conclusion

We have been able to correlate experimentally the structure of the nanotubular J-aggregates with the orientations of the excitonic transitions. It is of special significance that the J-aggregate band at 489 nm contributes to the charge transfer necessary for the screening of perpendicular radiation, generating a strong structure-induced anisotropy in the polarizability. This is a second level of anisotropy that is generated by the rolling of the porphyrin sheet into a quasi-one dimensional nanotube and that is enhanced by the assembly in bundles . However, the porphyrin sheet already contains directions of anisotropy given by the mutually orthogonal H- and J- excitonic transitions. Series of polarimetric transmission and scattering measurements have allowed us to discern among absorption and scattering contributions to

the extinction and, therefore, parse the two levels of anisotropy in these self-assembled nanostructures.

The porphyrin nanotubes act as excitonic antennas or photon concentrators for visible light with the particularity that they have both, axial and radial, transitions allowed in the structure. This is a unique characteristic when compared to other one-dimensional materials, such as inorganic nanowires or carbon nanotubes and it represents a clear advantage to funnel the photon excitations towards specific locations, especially when they assemble in large bundles. Future efforts should focus on the preparation of oriented collective nanoparticle microstructures (for example by the alignment with microflow techniques) and on inter-facing such antenna structures with optoelectronic devices to explore uses in photovoltaics and photodetectors.

## Acknowledgements

## References

1 T. Kobayashi, *J-aggregates. Volume 2*, World Scientific, Singapore.

2 F. Würthner, T. E. Kaiser and C. R. Saha-Möller, *Angew. Chem. Int. Ed.*, 2011, **50**, 3376–3410.

3 B. J. Walker, *PhD thesis*, Massachusetts Institute of Technology, 2011.

4 P. J. Collings, E. J. Gibbs, T. E. Starr, O. Vafek, C. Yee, L. A. Pomerance and R. F. Pasternack, *J. Phys. Chem. B*, 1999, **103**, 8474–8481.

5 N. Micali, F. Mallamace, A. Romeo, R. Purrello and L. Monsù Scolaro, *J. Phys. Chem. B*, 2000, **104**, 5897–5904.

6 D. M. Eisele, D. H. Arias, X. Fu, E. A. Bloemsma, C. P. Steiner, R. A. Jensen, P. Rebentrost, H. Eisele, A. Tokmakoff, S. Lloyd, K. A. Nelson, D. Nicastro, J. Knoester and M. G. Bawendi, *Proceedings of the National Academy of Sciences*, 2014, **111**, E3367–E3375.

7 Y. Wan, A. Stradomska, S. Fong, Z. Guo, R. D. Schaller, G. P. Wiederrecht, J. Knoester and L. Huang, *The Journal of Physical Chemistry C*, 2014, **118**, 24854–24865.

8 F. C. Spano and C. Silva, *Annual Review of Physical Chemistry*, 2014, **65**, 477–500.

9 Z. El-Hachemi, C. Escudero, F. Acosta-Reyes, M. T. Casas, V. Altoe, S. Aloni, G. Oncins, A. Sorrenti, J. Crusats, J. L. Campos and J. M. Ribo, *J. Mater. Chem. C*, 2013, **1**, 3337–3346.

10 O. Ohno, Y. Kaizu and H. Kobayashi, *The Journal of Chemical Physics*, 1993, **99**, 4128–4139.

11 O. Arteaga, C. Escudero, G. Oncins, Z. El-Hachemi, J. Llorens, J. Crusats, A. Canillas and J. M. Ribó, *Chemistry - An Asian Journal*, 2009, **4**, 1687–1696.

12 S. C. M. Gandini, E. L. Gelamo, R. Itri and M. Tabak, *Biophysical Journal*, 2003, **85**, 1259–1268.

13 S. M. Vlaming, R. Augulis, M. C. A. Stuart, J. Knoester and

P. H. M. van Loosdrecht, *J. Phys. Chem. B*, 2009, **113**, 2273–2283.

14 J. M. Short, J. A. Berriman, C. Kübel, Z. El-Hachemi, J.-V. Naubron and T. S. Balaban, *ChemPhysChem*, 2013, **14**, 3209–3214.

15 O. Arteaga, J. Freudenthal, B. Wang and B. Kahr, *Appl. Opt.*, 2012, **51**, 6805–6817.

16 O. Arteaga, M. Baldrís, J. Antó, A. Canillas, E. Pascual and E. Bertran, *Appl. Opt.*, 2014, **53**, 2236–2245.

17 O. Arteaga and A. Canillas, *Opt. Lett.*, 2010, **35**, 559–561.

18 C. Escudero, Z. El-Hachemi, J. Crusats and J. M. Ribó, *J. Porphyrins Phthalocyanines*, 2005, **09**, 852–863.

19 R. F. Pasternack and P. J. Collings, *Science*, 1995, **269**, 935–939.

20 F. Tantussi, F. Fuso, M. Allegrini, N. Micali, I. G. Occhiuto, L. M. Scolaro and S. Patane, *Nanoscale*, 2014, **6**, 10874–10878.

21 E. Malic, A. Knorr and S. Winnerl, *Graphene and carbon nanotubes ultrafast relaxation dynamics and optics*, Wiley, 2013.

22 Y. Wang, K. Kempa, B. Kimball, J. B. Carlson, G. Benham, W. Z. Li, T. Kempa, J. Rybczynski, A. Herczynski and Z. F. Ren, *Applied Physics Letters*, 2004, **85**, 2607–2609.

23 E. Cubukcu, F. Degirmenci, C. Kocabas, M. A. Zimmler, J. A. Rogers and F. Capasso, *Proceedings of the National Academy of Sciences*, 2009, **106**, 2495–2499.

24 M. Y. Sfeir, F. Wang, L. Huang, C.-C. Chuang, J. Hone, S. P. O'Brien, T. F. Heinz and L. E. Brus, *Science*, 2004, **306**, 1540–1543.

25 J. J. Crochet, J. D. Sau, J. G. Duque, S. K. Doorn and M. L. Cohen, *ACS Nano*, 2011, **5**, 2611–2618.

26 O. Arteaga, A. Canillas, J. Crusats, Z. El-Hachemi, J. Llorens, E. Sacristan and J. M. Ribo, *ChemPhysChem*, 2010, **11**, 3511–3516.

27 O. Arteaga, A. Canillas, R. Purrello and J. M. Ribó, *Opt. Lett.*, 2009, **34**, 2177–2179.